Spectroscopic Signatures of AA′ and AB Stacking of Chemical Vapor Deposited Bilayer MoS_2

Ming Xia,[†] Bo Li,[‡] Kuibo Yin,[§,∥] Giovanni Capellini,[⊥] Gang Niu,[⊥] Yongji Gong,[‡] Wu Zhou,[∥] Pulickel M. Ajayan,[‡] and Ya-Hong Xie*[,†]

[†]Department of Materials Science and Engineering, University of California, Los Angeles, California 90095, United States, [‡]Department of Materials Science and NanoEngineering, Rice University, Houston, Texas 77005, United States, [§]SEU-FEI Nano-Pico Center, Key Laboratory of MEMS of Ministry of Education, Southeast University, Nanjing 210096, China, [∥]Materials Science and Technology Division, Oak Ridge National Laboratory, Oak Ridge, Tennessee 37831, United States, and [⊥]Innovations for High Performance (IHP), ImTechnologiepark 25, Frankfurt D-15236, Germany

ABSTRACT Prominent resonance Raman and photoluminescence spectroscopic differences between AA′ and AB stacked bilayer molybdenum disulfide (MoS_2) grown by chemical vapor deposition are reported. Bilayer MoS_2 islands consisting of the two stacking orders were obtained under identical growth conditions. Resonance Raman and photoluminescence spectra of AA′ and AB stacked bilayer MoS_2 were obtained on Au nanopyramid surfaces under strong plasmon resonance. Both resonance Raman and photoluminescence spectra show distinct features indicating clear differences in interlayer interaction between these two phases. The implication of these findings on device applications based on spin and valley degrees of freedom will be discussed.

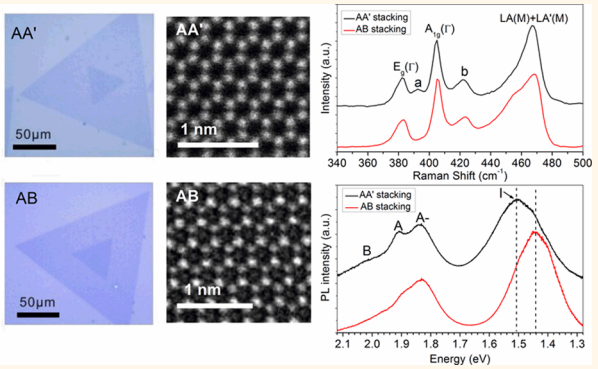

KEYWORDS: molybdenum disulfide · bilayer stacking · Au nanopyramids · photoluminescence · resonance Raman

Molybdenum disulfide (MoS_2) is a member of layered transition metal dichalcogenides (TMDs) with a number of highly interesting physical properties. The indirect band gap of 1.2 eV in the bulk form evolves with a decreasing number of layers and becomes a direct band gap of 1.9 eV in monolayer MoS_2.[1−3] In many senses, the most unique property of the TMD family of materials consisting of combinations of Mo, W, S, and Se is the strong spin−orbit coupling.[4] This originates from the d-orbitals of the heavy elements (Mo and W)[5] and offers exciting opportunities for device applications, leveraging spin and valley degrees of freedom.[6−8] Compared to the more studied monolayer TMDs, bilayer structures offer an added layer degree of freedom. Interactions between MoS_2 layers as well as the specific stacking order can significantly modify their electrical,[9] optical,[3] and vibrational properties.[10] The specific spin−orbit-based behavior depends sensitively on crystal symmetry, as elucidated by many theoretical studies.[4,11] Robust valley polarization is assured by the lack of centrosymmetry in all monolayer TMDs as well as bilayer ones with AB stacking.[6] Furthermore, interlayer hopping has been shown to be significantly suppressed by the strong coupling between spin and valley pseudospin as well as layer pseudospin,[12−14] allowing for the signatures of different spin, valley, and layer states to be experimentally observed. Finally, the coherent lengths of a given symmetry are determined by material imperfections with some being intrinsic to the method of fabrication, including chemical vapor deposition (CVD)[15] and exfoliation.[3] We report the results of combined optical spectroscopy and electron microscopy studies on AA′ and AB stacked bilayer MoS_2 shedding light on potential challenges of device applications based on spin and valley degrees of freedom.

Many insightful experimental studies have appeared in the literature in the past couple of years.[6−8,16,17] Recent study[6,18] on

* Address correspondence to yhx@ucla.edu.

Received for review August 31, 2015 and accepted November 4, 2015.

Published online 10.1021/acsnano.5b05474

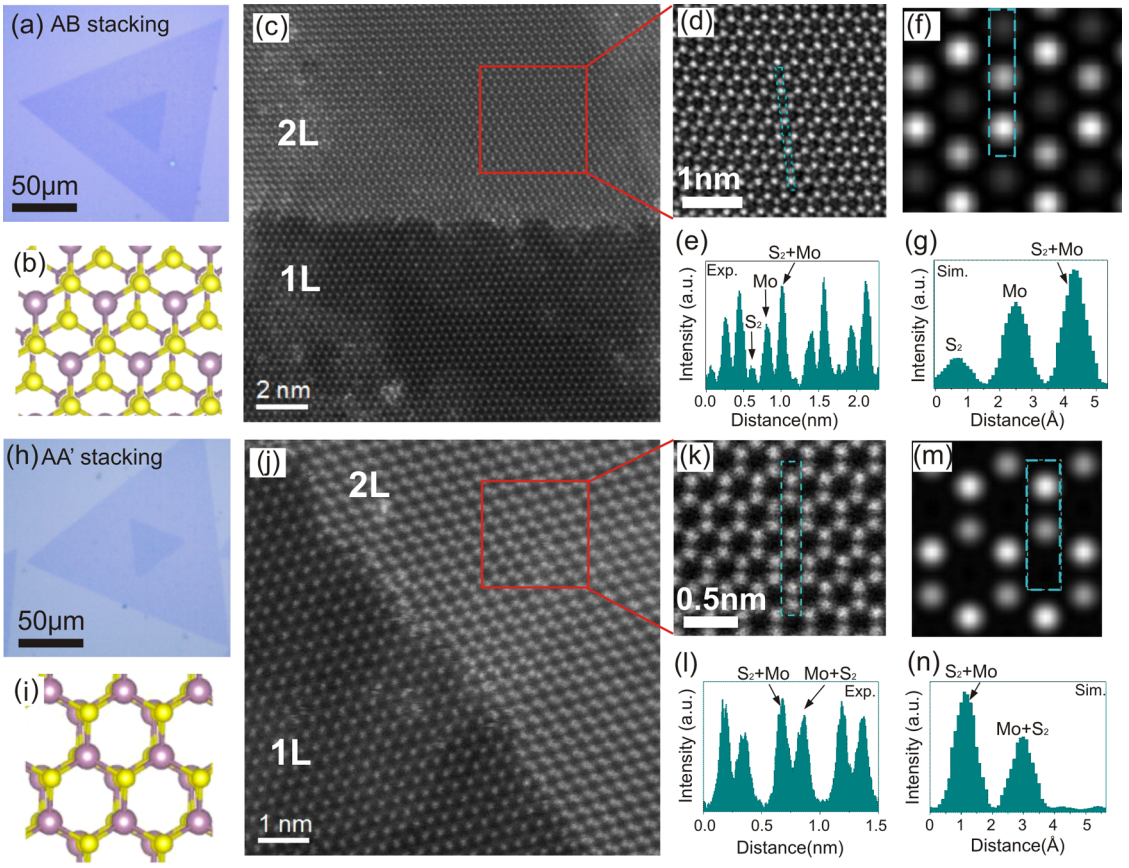

Figure 1. (a) Optical image and (b) atomic configuration of AB stacked bilayer MoS_2. (c) STEM-HAADF image of the boundary between AB stacked bilayer and monolayer MoS_2. (d) Magnified image of the red-boxed area in (c). (e) Intensity profile of the selected line (bright cyan) in (d). (f) Simulated STEM-HAADF image and (g) simulated intensity profile of the selected line (bright cyan) in (f). (h) Optical image and (i) atomic configuration of AA′ stacked bilayer MoS_2. (j) STEM-HAADF image of the boundary between AA′ stacked bilayer and monolayer MoS_2. (k) Magnified image of the red-boxed area in (j). (l) Intensity profile of the selected line (bright cyan) in (k). (m) Simulated STEM-HAADF image and (n) simulated intensity profile of the selected line (bright cyan) in (m). Purple balls in (b) and (i) represent Mo atoms, and yellow balls represent S atoms.

spin-polarization in MoS_2 also addressed the importance of stacking order between the adjacent MoS_2 layer on the spin/valley polarization. Interlayer interaction between adjacent MoS_2 layers with different stacking order has been investigated by stacking two CVD-grown monolayer MoS_2 with a range of different twisting angles[19,20] or CVD-grown bilayer MoS_2.[21] These reports show clear stacking angle dependence of the optical properties of bilayer MoS_2.[19−21] However, in these reports, there is no mention of the spectral differences between bilayer MoS_2 with 0 and 60° stacking angles, which correspond to the natural phases of MoS_2, 3R and 2H, respectively.[19] To date, only one of the experimental results[16] showed the difference between the photoluminescence (PL) spectra of 2H and 3R bulk MoS_2 with Cl_2 molecules intercalated between MoS_2 layers. We present for the first time (to the best of our knowledge) combined spectroscopy studies of bilayer MoS_2 of 0° (AB stacking) and 60° stacking (AA′ stacking) with clear differences in both Raman and PL spectra. The studies were enabled by the drastically enhanced signal-to-noise (S/N) ratios derived from plasmon resonance.

RESULTS AND DISCUSSION

Bilayer MoS_2 with different stacking orders in this study was grown by CVD[15] and transferred on a Au plasmonic surface for optical studies. The plasmonic surface used in the experiment is a Au nanopyramid structure, which was fabricated by sphere lithography.[22] Plasmon resonance on the Au nanopyramid surface has been shown to enhance the Raman signal of molecules by up to 7 orders of magnitude.[22,23] Another unique feature of the Au nanopyramid plasmonic surface is the out-of-plane electric field component of nearly the same intensity as that in the in-plane component near the Au pyramid surface (Figure S6).

CVD-grown bilayer MoS_2 in our experiments typically shows two kinds of microscopic shapes, one with a 0° twist angle between the two layers (AB stacking) and the other with a 60° twist angle (AA′ stacking), as shown in Figure 1a,h, respectively. Although many theoretical studies[18,24] have illustrated the possible atomic configurations in bilayer MoS_2 with the two different stacking orders, few experiments have been done on an atomic scale. In this study, scanning

transmission electron microscopy (STEM) was employed to establish the correlation between the atomic arrangement and the microscopic shape of the bilayer islands. The contrast of the STEM high-angle annular dark-field (STEM-HAADF) image is sensitive to the atomic number and sample thickness, which makes it possible to identify the detailed atomic arrangement. Figure 1c,j shows two typical STEM-HAADF images of the boundary regions between monolayer and bilayer MoS_2. The Mo and S atoms in the monolayer can be unambiguously distinguished due to their obvious large difference in atomic numbers. To correctly interpret our bilayer STEM images, the QSTEM simulation package[25,26] was employed. By comparing the experimental with the simulated STEM images, we can deduce the real atomic configurations of the bilayer MoS_2 samples. Figure 1d is the enlarged red-boxed region of the experimental image from the bilayer region of the sample with a 0° twist angle, as shown in Figure 1c. Figure 1f is the simulated STEM image of the atomic configuration shown in Figure 1b, that is, the AB stacked bilayer MoS_2. It can be seen that Figure 1f is identical to Figure 1d. Furthermore, the experimental intensity profile shown in Figure 1e is nearly identical to the simulated intensity profile shown in Figure 1g. Therefore, it can be deduced that Figure 1d has the same atomic configuration as shown in Figure 1b, that is, the AB stacked bilayer MoS_2. In the same way, we can get that Figure 1k, the enlarged red-boxed region of the experimental image from the bilayer region of the sample with a 60° twist angle, as shown in Figure 1j, has the same atomic configuration as shown in Figure 1i, that is, the AA′ stacked bilayer MoS_2. It is worth noting that more than one atomic configuration was found in the same bilayer sample due to relative shifting of the two layers, as shown in Figure S7. Our STEM results lend strong support to the assignment that the bilayer MoS_2 with a 0° twist angle is of AB stacking order whereas that with a 60° twist angle is of AA′ stacking order.

Raman spectroscopy has proven to be a powerful tool to study the optical response of 2D van der Waals materials such as graphene.[27] For MoS_2 atomic layers, Raman spectroscopy shows a clear evolution trend of A_{1g} and E^1_{2g} peak positions with layer thickness.[10,28] As layer thickness increases, the A_{1g} peak position blue shifts while the E^1_{2g} peak red shifts.[10,28] Compared with the first-order process in normal Raman scattering, resonance Raman scattering enhances the possibility of higher-order Raman scattering resulting in enriched spectral information. Resonance Raman scattering happens for a system when the incident laser excitation energy overlaps with (or is close to) the electronic band gap energy. In this study, the resonance condition was achieved by exciting the sample with a 633 nm laser (1.96 eV photon energy). Previous resonance Raman study of atomically thin MoS_2 layers at room temperature[29] suffers from a low signal-to-noise ratio due to the typically low Raman yield. This shortcoming of Raman spectroscopy can be overcome with the help of surface plasmon resonance, that is, surface-enhanced Raman spectroscopy (SERS). In our study, we employ a specific type of plasmonic surface, Au nanopyramid plasmonic substrates (Figure 2b), to boost the Raman signal of MoS_2 layers.

The resonance Raman spectra of AA′ and AB stacked bilayer MoS_2 measured on Au nanopyramid substrates are shown in Figure 2a. The inset optical image in Figure 2a shows two types of bilayer MoS_2 on Au nanopyramid substrates. Two major peaks, E_g (385 cm^{-1}) and A_{1g} (405 cm^{-1}), can be identified in the spectra. The E_g symmetry band in the AA′ stacked bilayer corresponds to the E_{2g} symmetry band in the 2H bulk MoS_2.[30] The E_g peak represents vibration of Mo and S atoms in the basal plane, whereas in the A_{1g} vibrational configuration, Mo atoms remain fixed and only S atoms vibrate along the *c*-axis. The new Raman peaks, which are not commonly observed with the 514 or 532 nm laser lines, are assigned based on resonant Raman of bulk MoS_2.[17] The Raman peak at 179 cm^{-1} is assigned to a difference combination mode of $A_{1g}(M) - LA'(M)$, where the LA′(M) mode (233 cm^{-1}) is a quasi-longitudinal acoustic (LA′) mode at the M point of Brillouin zone.[17] The peak at 420 cm^{-1}, commonly known as "b" peak, is assigned to a two-phonon process, and the appearance of this mode is related to the A exciton at the K point.[31] The peak located at ~460 cm^{-1} is asymmetrical and can be viewed as being composed of two parts. The lower frequency part of this peak is due to a van Hove singularity between the K and M points of the Brillouin zone, and the higher frequency part is mostly due to the LA and LA′ phonons at the M point. The peaks at 526, 571, 599, and 642 cm^{-1} are assigned to $E_g(M) + TA'(M)$, $A_{1g}(M) + TA'(M)$, $E_g(M) + LA'(M)$, and $A_{1g}(M) + LA'(M)$, respectively. TA′(M) is a quasi-transverse acoustic (TA′) mode at the M point of the Brillouin zone. For comparison, resonance Raman spectra of MoS_2 on a flat Au surface and SiO_2/Si substrates are shown in Figure 2d. The S/N ratios of Raman spectra of MoS_2 on both flat Au surface and SiO_2/Si substrates are lower than those on Au nanopyramids. It can be seen that the major Raman peak positions and shapes of MoS_2 on the flat Au surface are similar to those on Au nanopyramids. Although the Raman spectral shapes of AA′ and AB stacked bilayer MoS_2 on SiO_2/Si substrates appear to be different, these features vary among different samples with the same stacking order. As such, the Raman spectral shape is not an identifying feature of the MoS_2 stacking order. SERS enhancement factors (EFs) calculated for MoS_2 bilayer are on the order of 10^5 (see details in the Supporting Information). SERS EF represents the extent the Raman signal is boosted compared to regular Raman. In this study,

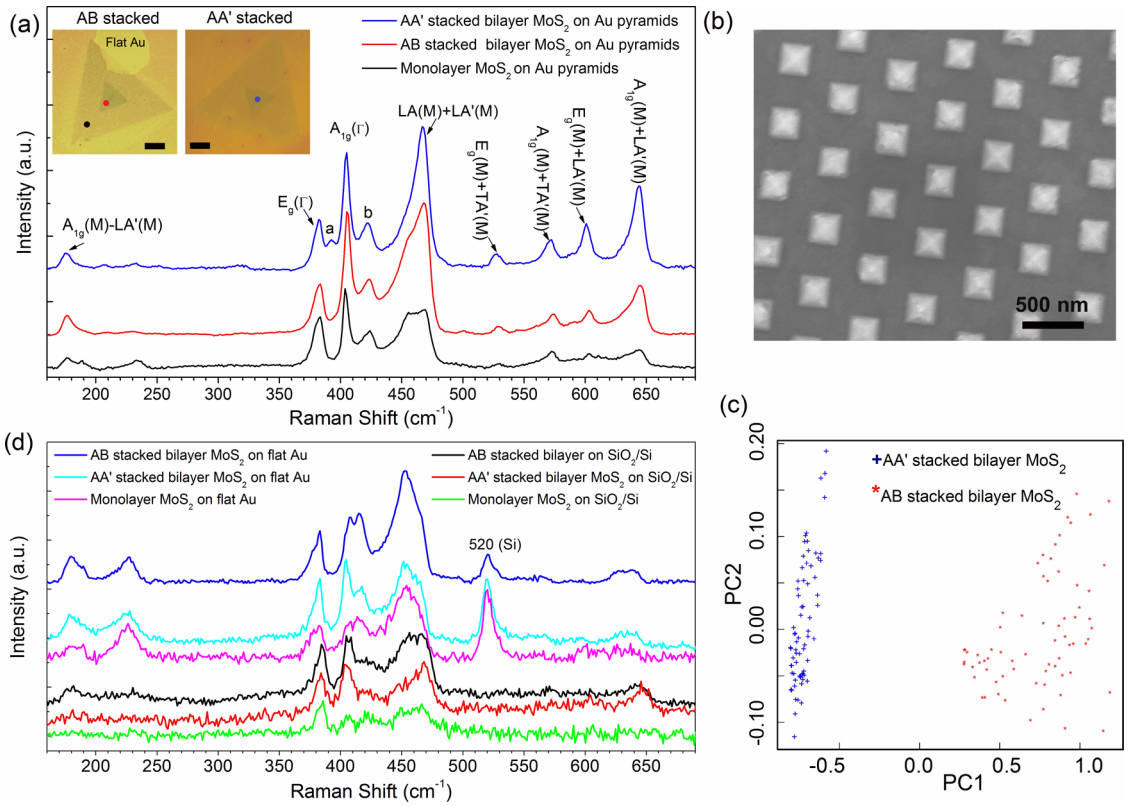

Figure 2. (a) Resonance Raman spectra of monolayer and bilayer MoS_2 on Au nanopyramids. The blue, red, and black spectra were obtained at the spots with the same color in the samples shown in the inset optical image. The inset optical image shows the AA′ and AB stacked bilayer MoS_2 on Au nanopyramids (the Au nanopyramid substrates contain some interdispersed flat Au regions). The scale bars in the inset image are 50 μm. (b) SEM image of Au nanopyramid SERS substrate. (c) PCA diagram of AA′ and AB stacked bilayer MoS_2 resonance Raman data. (d) Resonance Raman spectra of monolayer and bilayer MoS_2 on flat Au substrates and SiO_2/Si substrates. The Raman spectra were measured at 300 K.

SERS enhancement is mainly due to the electromagnetic (EM) enhancement mechanism. As such, SERS EF could be used as a figure of merit to measure the extent of plasmon resonance of Au nanopyramids referenced to either the flat Au surface or the SiO_2 surface.

The high S/N ratio renders clear spectral differences between AA′ and AB stacked bilayer MoS_2. The primary difference is the appearance of the 395 cm^{-1} peak in the AA′ stacked bilayer MoS_2. Among all the bilayer samples (more than 10 samples for each phase) measured, the 395 cm^{-1} peak only appears in Raman spectra of AA′ stacked bilayer, never in those of the AB stacked bilayer. More Raman spectra of bilayer samples can be found in Figure S4. This 395 cm^{-1} mode has been observed for 2H bulk MoS_2 using resonance Raman spectroscopy at low temperature and was named "a" peak.[32,33] Livneh *et al.*[17,32] found that in bulk MoS_2 this mode is constructed from two contributions, which are particularly distinguishable at low temperatures. The two contributions that construct "a" mode are assigned as LA′(M) + TA′(M) and LA(M) + TA(M).[17] To obtain a quantifiable measure of the spectral differences, we employed principal component analysis (PCA).[34] PCA is a statistical procedure widely used in analyzing Raman spectra to identify spectral differences between data sets. PCA transforms the dimensionality of a data matrix (*e.g.*, intensity *versus* wavenumber) to a new set of orthogonal variables that have the strongest correlations with distinctive spectral features. The new set of variables is known as principal components (PCs). Plots of one PC against another provide quantitative information about how different the data sets are in terms of sensitivity, specificity, *etc.* Figure 2c shows the PCA diagram of bilayer MoS_2 resonance Raman data. It can be seen that the Raman data corresponding to the two different stacking orders are distinctively different in the space of principal components.

To study the variation of the "a" peak within one bilayer sample, Raman mapping was conducted. Figure 3b,d shows the stacked resonance Raman spectra measured from AA′ (Figure 3a) and AB stacked bilayer samples (Figure 3c) at room temperature, respectively. Among the spectra measured from the AA′ stacked bilayer sample, the "a" peak always exists. However, this peak never appears in any of the AB stacked bilayer resonance Raman spectra. We also conducted variable-temperature Raman measurements of bilayer MoS_2 on the Au nanopyramid structure. As shown in Figure 4, the key features of the bilayer Raman spectra do not show noticeable temperature

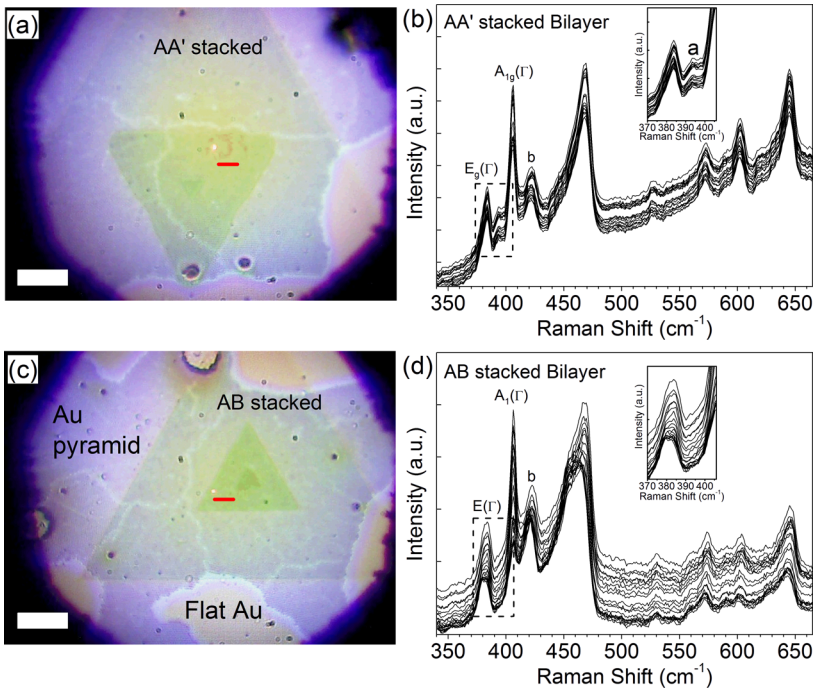

Figure 3. (a) Optical image of a AB stacked bilayer MoS_2 sheet on Au nanopyramids. (b) Raman spectra obtained from line mapping (red line in (a)) with *z*-axis offset. (c) Optical image of a AA′ stacked bilayer MoS_2 sheet on Au nanopyramids. (d) Raman spectra obtained from line mapping (red line in (c)) with *z*-axis offset. The meandering lines and other features in the background are due to the inhomogeneity of our nanopatterning process. The scale bars in (a) and (c) are 10 μm. The Raman spectra shown in (b) and (d) are original spectra without background subtraction and were measured at 300 K. The inset figures in (b) and (d) are the enlarged spectra between 370 and 410 cm^{-1}. It can be seen that "a" peak appears only in the AA′ stacked bilayer sample.

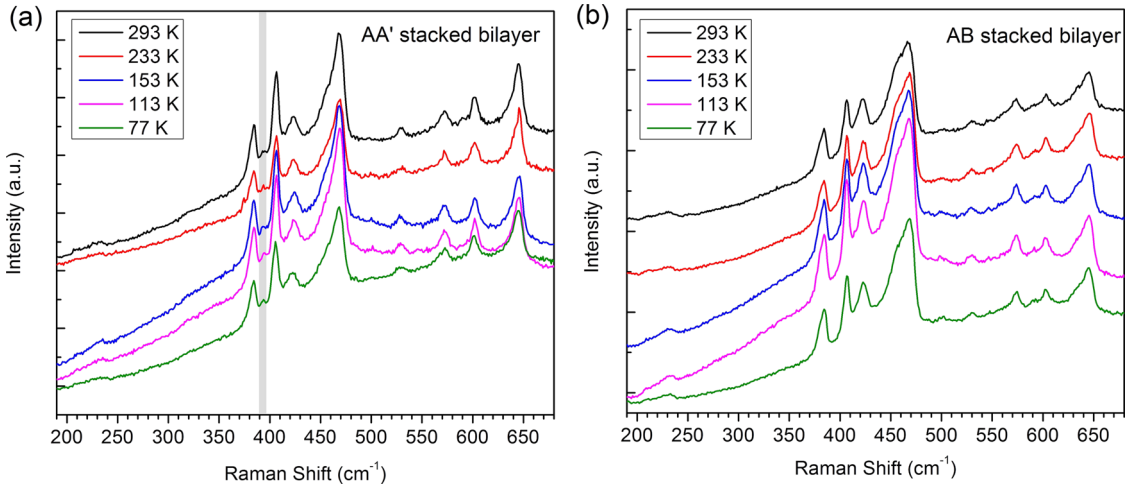

Figure 4. Resonance Raman spectra of (a) AA′ and (b) AB stacked bilayer MoS_2 on a Au nanopyramid substrate at different temperatures. Gray bar in (a) indicates the position of "a" peak.

dependence. More importantly, the "a" mode persists in the AA′ (2H or 60° stacking) stacked bilayer at temperatures ranging from 293 to 77 K but remains absent from the AB (3R or 0° stacking) stacked bilayer across the same temperature range. Interestingly, for AA′ stacked bilayer MoS_2, we did not observe that "a" peak separated into two parts as temperature decreased from 293 to 77 K, which was different from the situation for 2H bulk MoS_2.[17] This may be due to the reduced symmetry of AA′ stacked bilayer MoS_2 (D_{3d}) compared with that of 2H bulk MoS_2 (D_{6h}). Considering that the "a" peak position is located at ~395 cm^{-1} in our case, it could be assigned as TA′(M) + LA′(M) according to ref 17. The SERS results suggest that this "a" peak could act as a Raman fingerprint to differentiate the two types of MoS_2 bilayers. A quantitative understanding of the Raman spectral differences would require theoretical calculations of phonon

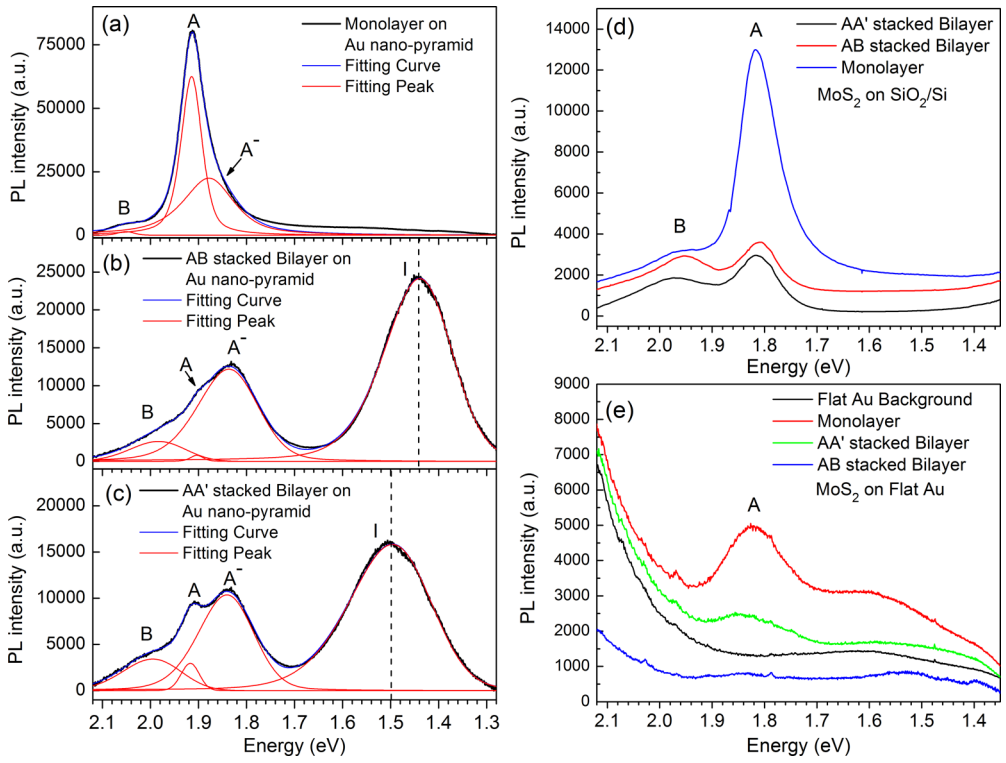

Figure 5. PL spectra of MoS_2 on Au nanopyramid substrates: (a) monolayer MoS_2, (b) AB stacked bilayer MoS_2, and (c) AA′ stacked bilayer MoS_2. (d) PL spectra of MoS_2 on SiO_2/Si substrates. (e) PL spectra of MoS_2 on flat Au substrates. A 532 nm laser (0.8 mW power) was used for PL measurement at 300 K.

dispersion and density of states for two different MoS_2 phases. We hope that our results will motivate such calculations in the future. Our findings provide two additional methods (in addition to low-temperature photoluminescence[16]) for definitive determination of bilayer MoS_2 stacking orders, namely, optical microscopy for isolated islands and SERS.

In addition to the phonon vibrations, the electronic band structure of MoS_2 bilayers was investigated using PL. PL spectra of both monolayer and bilayer MoS_2 on Au nanopyramids are shown in Figure 5a–c. The A and B peaks represent the direct gap transitions, and the I peak in bilayer MoS_2 PL spectra represents the indirect gap transition. The A^- peak is the trion peak.[20,35] The Au nanopyramid substrate enhances the PL peak intensity by 2 orders of magnitude compared with PL of MoS_2 on a flat Au surface (Figure 5e) and by almost 1 order of magnitude compared with that on the SiO_2/Si substrate (Figure 5d). It is also observed that the peak intensity of the MoS_2 PL spectra measured on the SiO_2/Si substrate is higher than those on a flat Au surface. In the PL spectra of MoS_2 on both a flat Au surface and a SiO_2 surface, the A^- peak is not clearly observed, and the I peak intensity of the bilayer is very weak and nondiscernable compared with the strong I peak intensity observed on the Au nanopyramid substrate. The physical origin of the strong I peak intensity observed on the Au nanopyramid substrate is yet to be understood and warrants further studies.

The enhanced S/N ratio provided by the Au-tipped surface allows for the observation of more spectral details. The most prominent difference between monolayer and bilayer MoS_2 is the strong I peak in bilayer MoS_2. For bilayer MoS_2, the primary PL spectral difference between AA′ and AB stacked bilayer is the I peak position. A noticeable blue shift of the I peak of AA′ stacked bilayer by 0.056 ± 0.017 eV over that of the AB stacked bilayer was observed. This observation agrees with the density functional theory (DFT) calculation findings of He *et al.*[9] in terms of the general trend but being different in value (0.06 eV from our PL study *versus* 0.14 eV from DFT calculations). Previous experimental results[19,21] did not address the difference between the I peak positions of AA′ and AB stacked bilayer MoS_2. In addition, the I/A peak intensity ratio in PL spectra obtained on a Au pyramid region is higher than that in the previous experiment results obtained on SiO_2/Si substrates.[19,21] The emergence of the indirect band gap results from the interlayer electronic coupling. In the bilayer MoS_2 band structure, the doubly degenerate valence band splits into more branches near the Γ point, and the upper branch reaches an energy value higher than the valence band at the K point in monolayer MoS_2. It has been suggested that the indirect band gap being an indicator of the interlayer electronic coupling strength with lower the indirect band gap, which correlates to a higher coupling strength.[21] Our PL results indicate stronger

interlayer electronic coupling in AB stacked bilayer MoS_2 over that of AA′ stacked bilayer. The electronic coupling is significantly affected by the separation between layers.[21] It is mainly defined by the orbital overlap of the inner sulfur atoms from the adjacent MoS_2 layers,[19] with a smaller interlayer distance leading to stronger electronic coupling.[19,21] Both DFT calculation[9,19] and experimental data[36] show that AB stacked bilayer MoS_2 has an interlayer distance smaller than that in the AA′ stacked bilayer. These findings support our finding. The difference between indirect gap energy in the two MoS_2 phases can also be understood from the perspective of electronic band splitting. DFT simulation results[9] show that AB stacked bilayer MoS_2 has an additional band splitting over that of the AA′ stacked bilayer. Because of the lack of centro-symmetry in AB stacking, four bands are formed (instead of two in AA′ stacking) along the M−K−Γ direction in the AB stacked bilayer Brillouin zone. The band splitting causes a lower indirect band gap in the AB stacked bilayer MoS_2.

It can be noticed from Figure 5b,c that A^-/A peak intensity ratio of PL spectra of AA′ and AB stacked bilayer MoS_2 is different. However, this peak intensity ratio is not unique to AA′ or AB stacking. The A^-/A peak intensity ratio fluctuation can be observed in both AA′ and AB stacked bilayer samples. As such, it is not an identifying feature of the stacking order. In the search for the physical origin of the observed fluctuation of the A^-/A peak ratio in PL, we note two features unique to our Au-tipped surfaces. The first one is the tensor nature of the plasmonic surface. Plasmon resonance transforms the TE mode of the excitation light of near perpendicular incidence (with the electric field vector being coplanar with MoS_2 layers) into a local electromagnetic (EM) field, with the out-of-plane electric field being comparable to the in-plane field (Figure S8b). The out-of-plane electric field component contributes to symmetry breaking that could lead to noticeable changes in the luminescence behavior of especially the symmetric AA′ stacked islands. The second feature is the difference in electron affinity between Au (2.308 eV)[37] and bilayer MoS_2 (4.0−4.2 eV),[38−40] leading to an effective n-type doping of MoS_2.[41] Considering the Au and the MoS_2 as two equal potential bodies, the electron density in MoS_2 will be dependent on the distance between it and the underlying Au surface, which in turn varies with location due to the imperfection in our nanofabrication. The exciton and trion luminescence peak intensities are known to depend sensitively and differently on the local carrier density.[35] This we believe is the reason for the variation observed in the A^-/A peak ratio.

It can also be noticed that there is a slight blue shift of the A peak from the monolayer and bilayer MoS_2 on the Au pyramid region compared with those on the flat Au region and on the SiO_2/Si substrate. The origin of the blue shift cannot be explained by the static electric field due to the electron transfer from Au to MoS_2 because of the red shift predicted by DFT simulation.[42,43] There are two main differences in the physical environment of MoS_2 over Au pyramids compared to that over flat Au: the tensile strain in MoS_2 due to the nonplanar topology of the Au pyramids and the significant out-of-plane EM field due to plasmon resonance. The former is unlikely to be the primary cause based on the previous experimental observations of tensile strain leading to the PL red shift.[44,45] By the process of elimination, we believe that the primary cause of the A peak blue shift is the intense out-of-plane EM field from the plasmon resonance. Further study is needed to confirm this point.

Considering the growing interest in valleytronics in TMD materials, the interlayer stacking order is definitely a key variable which should be considered when developing valleytronics technology. It has been proven that AB stacked bilayer MoS_2 can provide valley polarization more robust than that of the AA′ stacked bilayer due to the non-centro-symmetry.[6] Therefore, one primary concern is to control the fabrication so that only one type (AB stacking) of stacking is present. AA′ stacked (2H phase) MoS_2 is dominant and more stable in nature. 3R MoS_2 has been shown to transform to 2H MoS_2 at increased temperatures.[46] The histogram of our CVD-grown samples shows that AA′ stacked bilayer islands outnumber that of AB stacked bilayer by almost 50% (∼370 over ∼250 as in Figure S10). DFT calculation also indicates that AA′ stacked bilayer MoS_2 has a ground state total energy relatively lower than that of the AB stacked bilayer.[9] It is apparent that the ability of fabricating exclusively AB stacked bilayer MoS_2 appears to be a fundamental challenge and requires in-depth understanding of the most manufacturable fabrication technology, CVD.

CONCLUSION

We have demonstrated that the CVD grown AA′ (60° stacking) and AB (0° stacking) stacked bilayer MoS_2 have distinct properties in terms of Raman and PL using Au nanopyramid plasmonic substrates. The "a" peak appears in AA′ stacked bilayer MoS_2 resonance Raman spectra but not in the AB stacked bilayer, a feature that can be used as a Raman fingerprint to differentiate the two types of bilayer MoS_2. The lower indirect gap energy indicates that AB stacked bilayer MoS_2 has an interlayer electronic coupling stronger than that for the AA′ stacked bilayer. In addition to revealing the subtle differences in AA′ and AB stacked bilayer MoS_2, our results establish three methods for distinguishing between the two stacking orders, namely, optical microscopy, SERS, and PL. Considering the recent surge in interest in spin/valley polarization

of TMDs,[6−8] it is clear that understanding and controlling interlayer stacking is going to be a crucial variable that must be taken into account during device design.

METHODS

Au Nanopyramid Fabrication. Au nanopyramids were fabricated based on the sphere lithography method (see details in the Supporting Information). Periodic inverted silicon pyramidal pits, which are templated from close-packed monolayer colloidal crystals, are employed as structural templates to replicate arrays of Au nanopyramids.

MoS_2 Bilayer Sample Preparation. MoS_2 bilayer was prepared using the same method reported in ref 15. To synthesize MoS_2 atomic layers in a vapor phase deposition process, MoO_3 and pure sulfur were used as precursor and reactant materials, respectively. SiO_2/Si (300 nm thick SiO_2) substrates were used. CVD depositions were performed at the reaction temperature of 850 °C. Bilayer MoS_2 was transferred onto a Au-tipped surface *via* a standard PMMA-based transfer approach. MoS_2 bilayer samples on SiO_2/Si substrates were spin-coated with a PMMA layer (950 PMMA A4 from Microchem) with a spinning speed of 2000 rpm for 1 min and submerged in KOH solution. Subsequently, PMMA/MoS_2 film was cleaned by DI water and then transferred onto a Au-tipped surface. To avoid MoS_2 layers from being washed away, the PMMA layer (about 200 nm thickness) was not removed from the transferred MoS_2. STEM samples were prepared using a method similar to that used in the MoS_2/Au pyramid sample. The only difference was that the PMMA protecting layer was removed with acetone following the transfer.

STEM Analyses. STEM experiments were performed with the Nion UltraSTEM, a dedicated STEM equipped with a cold field emission electron source and a corrector of third and fifth order aberrations, operating at 60 kV accelerating voltage.

PL Measurement Setup. The micro-PL measurements were performed in backscattering geometry using a CW laser at 532 nm wavelength and a 50× IR objective lens of $N = 0.65$ numerical aperture (Olympus microscope). The excitation power at the sample surface was in the 0.5−2 mW range. Sample temperature was kept at 300 K using a Linkam cryostat. PL emission was dispersed by a Horiba iHR320 spectrometer and detected by a 256 × 1024 pixel Si CCD detector. The spectrometer was calibrated daily against reference emission and laser satellites. PL data have been normalized to the spectral response of the entire experimental setup measured by means of a calibrated light source.

Raman Measurement Setup. Raman spectra was measured using a Renishaw inVia microscope under 633 nm laser excitation. The laser power used was 0.5 mW. The grating used was 1800 l/mm, and the objective lens used was 100×. A step size of 200 nm was used for Raman mapping. Raman data were analyzed using Renishaw WiRE 3.2 software (see details in the Supporting Information).

Conflict of Interest: The authors declare no competing financial interest.

Supporting Information Available: The Supporting Information is available free of charge on the ACS Publications website at DOI: 10.1021/acsnano.5b05474.

Au nanopyramid preparation information; Raman data analysis method; SERS enhancement factors, FDTD simulation of electrical field distribution around Au nanopyramid substrate; Figures S1−S9 (PDF)

Acknowledgment. This work was supported in part by FAME, one of six centers of STARnet, a Semiconductor Research Corporation program sponsored by MARCO and DARPA. Y.-H.X. acknowledges the support from Alexander von Humboldt Foundation Research Award. Electron microscopy study was supported in part by the U.S. Department of Energy, Office of Science, Basic Energy Science, Materials Sciences and Engineering Division (K.Y, and W.Z), and through a user project at ORNL's Center for Nanophase Materials Sciences (CNMS), which is a DOE Office of Science User Facility. K.Y. acknowledges the scholarship from China Scholarship Council (No. 201208320383) and the support from National Natural Science Foundation of China (No. 11204034) and the Natural Science Foundation of Jiangsu Province (No. BK2012123).

REFERENCES AND NOTES

1. Mak, K. F.; Lee, C.; Hone, J.; Shan, J.; Heinz, T. F. Atomically Thin MoS_2: a New Direct-Gap Semiconductor. *Phys. Rev. Lett.* **2010**, *105*, 136805.
2. Eda, G.; Yamaguchi, H.; Voiry, D.; Fujita, T.; Chen, M.; Chhowalla, M. Photoluminescence from Chemically Exfoliated MoS_2. *Nano Lett.* **2011**, *11*, 5111–5116.
3. Splendiani, A.; Sun, L.; Zhang, Y.; Li, T.; Kim, J.; Chim, C.-Y.; Galli, G.; Wang, F. Emerging Photoluminescence in Monolayer MoS_2. *Nano Lett.* **2010**, *10*, 1271–1275.
4. Xiao, D.; Liu, G.-B.; Feng, W.; Xu, X.; Yao, W. Coupled Spin and Valley Physics in Monolayers of MoS_2 and Other Group-VI Dichalcogenides. *Phys. Rev. Lett.* **2012**, *108*, 196802.
5. Zhu, Z.; Cheng, Y.; Schwingenschlögl, U. Giant Spin-Orbit-Induced Spin Splitting in Two-Dimensional Transition-Metal Dichalcogenide Semiconductors. *Phys. Rev. B: Condens. Matter Mater. Phys.* **2011**, *84*, 153402.
6. Suzuki, R.; Sakano, M.; Zhang, Y.; Akashi, R.; Morikawa, D.; Harasawa, A.; Yaji, K.; Kuroda, K.; Miyamoto, K.; Okuda, T. Valley-Dependent Spin Polarization in Bulk MoS_2 with Broken Inversion Symmetry. *Nat. Nanotechnol.* **2014**, *9*, 611–617.
7. Zeng, H.; Dai, J.; Yao, W.; Xiao, D.; Cui, X. Valley Polarization in MoS_2 Monolayers by Optical Pumping. *Nat. Nanotechnol.* **2012**, *7*, 490–493.
8. Mak, K. F.; He, K.; Shan, J.; Heinz, T. F. Control of Valley Polarization in Monolayer MoS_2 by Optical Helicity. *Nat. Nanotechnol.* **2012**, *7*, 494–498.
9. He, J.; Hummer, K.; Franchini, C. Stacking Effects on the Electronic and Optical Properties of Bilayer Transition Metal Dichalcogenides MoS_2, $MoSe_2$, WS_2, and WSe_2. *Phys. Rev. B: Condens. Matter Mater. Phys.* **2014**, *89*, 075409.
10. Li, H.; Zhang, Q.; Yap, C. C. R.; Tay, B. K.; Edwin, T. H. T.; Olivier, A.; Baillargeat, D. From Bulk to Monolayer MoS_2: Evolution of Raman Scattering. *Adv. Funct. Mater.* **2012**, *22*, 1385–1390.
11. Wu, S.; Ross, J. S.; Liu, G.-B.; Aivazian, G.; Jones, A.; Fei, Z.; Zhu, W.; Xiao, D.; Yao, W.; Cobden, D. Electrical Tuning of Valley Magnetic Moment Through Symmetry Control in Bilayer MoS_2. *Nat. Phys.* **2013**, *9*, 149–153.
12. Zeng, H.; Liu, G.-B.; Dai, J.; Yan, Y.; Zhu, B.; He, R.; Xie, L.; Xu, S.; Chen, X.; Yao, W. Optical Signature of Symmetry Variations and Spin-Valley Coupling in Atomically Thin Tungsten Dichalcogenides. *Sci. Rep.* **2013**, *3*, 01608.
13. Gong, Z.; Liu, G.-B.; Yu, H.; Xiao, D.; Cui, X.; Xu, X.; Yao, W. Magnetoelectric Effects and Valley-Controlled Spin Quantum Gates in Transition Metal Dichalcogenide Bilayers. *Nat. Commun.* **2013**, *4*, 2053.
14. Xu, X.; Yao, W.; Xiao, D.; Heinz, T. F. Spin and Pseudospins in Layered Transition Metal Dichalcogenides. *Nat. Phys.* **2014**, *10*, 343–350.
15. Najmaei, S.; Liu, Z.; Zhou, W.; Zou, X.; Shi, G.; Lei, S.; Yakobson, B. I.; Idrobo, J.-C.; Ajayan, P. M.; Lou, J. Vapour Phase Growth and Grain Boundary Structure of Molybdenum Disulphide Atomic Layers. *Nat. Mater.* **2013**, *12*, 754–759.
16. Anghel, S.; Chumakov, Y.; Kravtsov, V.; Mitioglu, A.; Plochocka, P.; Sushkevich, K.; Volodina, G.; Colev, A.; Kulyuk, L. Identification of 2H and 3R Polytypes of MoS_2

Layered Crystals Using Photoluminescence Spectroscopy. *arXiv:1411.3850*, **2014**.
17. Livneh, T.; Spanier, J. E. A Comprehensive Spectral Analysis of Multiphonon Resonant Raman Scattering in 2H-MoS_2. *arXiv:1408.6748*, **2014**.
18. Jiang, T.; Liu, H.; Huang, D.; Zhang, S.; Li, Y.; Gong, X.; Shen, Y.-R.; Liu, W.-T.; Wu, S. Valley and Band Structure Engineering of Folded MoS_2 Bilayers. *Nat. Nanotechnol.* **2014**, *9*, 825–829.
19. van der Zande, A. M.; Kunstmann, J.; Chernikov, A.; Chenet, D. A.; You, Y.; Zhang, X.; Huang, P. Y.; Berkelbach, T. C.; Wang, L.; Zhang, F. Tailoring the Electronic Structure in Bilayer Molybdenum Disulfide *via* Interlayer Twist. *Nano Lett.* **2014**, *14*, 3869–3875.
20. Huang, S.; Ling, X.; Liang, L.; Kong, J.; Terrones, H.; Meunier, V.; Dresselhaus, M. S. Probing the Interlayer Coupling of Twisted Bilayer MoS_2 Using Photoluminescence Spectroscopy. *Nano Lett.* **2014**, *14*, 5500–5508.
21. Liu, K.; Zhang, L.; Cao, T.; Jin, C.; Qiu, D.; Zhou, Q.; Zettl, A.; Yang, P.; Louie, S. G.; Wang, F. Evolution of Interlayer Coupling in Twisted Molybdenum Disulfide Bilayers. *Nat. Commun.* **2014**, *5*, 4966.
22. Wang, P.; Zhang, W.; Liang, O.; Pantoja, M.; Katzer, J.; Schroeder, T.; Xie, Y. H. Giant Optical Response from Graphene-Plasmonic System. *ACS Nano* **2012**, *6*, 6244–6249.
23. Wang, P.; Liang, O.; Zhang, W.; Schroeder, T.; Xie, Y. H. Ultra-Sensitive Graphene-Plasmonic Hybrid Platform for Label-Free Detection. *Adv. Mater.* **2013**, *25*, 4918–4924.
24. Yang, S.; Kang, J.; Yue, Q.; Yao, K. Vapor Phase Growth and Imaging Stacking Order of Bilayer Molybdenum Disulfide. *J. Phys. Chem. C* **2014**, *118*, 9203–9208.
25. Koch, C. T. Determination of Core Structure Periodicity and Point Defect Density Along Dislocations. Ph.D. Thesis; Arizona State University, Phoenix, AZ, 2002.
26. Zhou, W.; Lee, J.; Nanda, J.; Pantelides, S. T.; Pennycook, S. J.; Idrobo, J.-C. Atomically Localized Plasmon Enhancement in Monolayer Graphene. *Nat. Nanotechnol.* **2012**, *7*, 161–165.
27. Ferrari, A. C.; Meyer, J. C.; Scardaci, V.; Casiraghi, C.; Lazzeri, M.; Mauri, F.; Piscanec, S.; Jiang, D.; Novoselov, K. S.; Roth, S.; et al. Raman Spectrum of Graphene and Graphene Layers. *Phys. Rev. Lett.* **2006**, *97*, 187401.
28. Lee, C.; Yan, H.; Brus, L. E.; Heinz, T. F.; Hone, J.; Ryu, S. Anomalous Lattice Vibrations of Single-and Few-Layer MoS_2. *ACS Nano* **2010**, *4*, 2695–2700.
29. Chakraborty, B.; Matte, H.; Sood, A.; Rao, C. Layer-Dependent Resonant Raman Scattering of a Few Layer MoS_2. *J. Raman Spectrosc.* **2013**, *44*, 92–96.
30. Scheuschner, N.; Gillen, R.; Staiger, M.; Maultzsch, J. Newly Observed First-Order Resonant Raman Modes in Few-Layer MoS_2. *arXiv:1503.08980*, **2015**.
31. Sekine, T.; Uchinokura, K.; Nakashizu, T.; Matsuura, E.; Yoshizaki, R. Dispersive Raman Mode of Layered Compound 2H-MoS_2 Under the Resonant Condition. *J. Phys. Soc. Jpn.* **1984**, *53*, 811–818.
32. Livneh, T.; Sterer, E. Resonant Raman Scattering at Exciton States Tuned by Pressure and Temperature in 2H-MoS_2. *Phys. Rev. B: Condens. Matter Mater. Phys.* **2010**, *81*, 195209.
33. Gołasa, K.; Grzeszczyk, M.; Leszczyński, P.; Faugeras, C.; Nicolet, A.; Wysmołek, A.; Potemski, M.; Babiński, A. Multiphonon Resonant Raman Scattering in MoS_2. *Appl. Phys. Lett.* **2014**, *104*, 092106.
34. Zhang, Z. M.; Chen, S.; Liang, Y. Z.; Liu, Z. X.; Zhang, Q. M.; Ding, L. X.; Ye, F.; Zhou, H. An Intelligent Background-Correction Algorithm for Highly Fluorescent Samples in Raman Spectroscopy. *J. Raman Spectrosc.* **2010**, *41*, 659–669.
35. Mak, K. F.; He, K.; Lee, C.; Lee, G. H.; Hone, J.; Heinz, T. F.; Shan, J. Tightly Bound Trions in Monolayer MoS_2. *Nat. Mater.* **2013**, *12*, 207–211.
36. Schönfeld, B.; Huang, J.; Moss, S. Anisotropic Mean-Square Displacements (MSD) in Single-Crystals of 2H-and 3R-MoS_2. *Acta Crystallogr., Sect. B: Struct. Sci.* **1983**, *39*, 404–407.
37. Andersen, T.; Haugen, H.; Hotop, H. Binding Energies in Atomic Negative Ions: III. *J. Phys. Chem. Ref. Data* **1999**, *28*, 1511–1533.
38. Han, S.; Kwon, H.; Kim, S. K.; Ryu, S.; Yun, W. S.; Kim, D.; Hwang, J.; Kang, J.-S.; Baik, J.; Shin, H. Band-Gap Transition induced by Interlayer van der Waals Interaction in MoS_2. *Phys. Rev. B: Condens. Matter Mater. Phys.* **2011**, *84*, 045409.
39. Choi, M. S.; Lee, G.-H.; Yu, Y.-J.; Lee, D.-Y.; Lee, S. H.; Kim, P.; Hone, J.; Yoo, W. J. Controlled Charge Trapping by Molybdenum Disulphide and Graphene in Ultrathin Heterostructured Memory Devices. *Nat. Commun.* **2013**, *4*, 1624.
40. Das, S.; Chen, H.-Y.; Penumatcha, A. V.; Appenzeller, J. High Performance Multilayer MoS_2 Transistors with Scandium Contacts. *Nano Lett.* **2013**, *13*, 100–105.
41. Fontana, M.; Deppe, T.; Boyd, A. K.; Rinzan, M.; Liu, A. Y.; Paranjape, M.; Barbara, P. Electron-Hole Transport and Photovoltaic Effect in Gated MoS_2 Schottky Junctions. *Sci. Rep.* **2013**, *3*, 1634.
42. Liu, Q.; Li, L.; Li, Y.; Gao, Z.; Chen, Z.; Lu, J. Tuning Electronic Structure of Bilayer MoS_2 by Vertical Electric Field: a First-Principles Investigation. *J. Phys. Chem. C* **2012**, *116*, 21556–21562.
43. Ramasubramaniam, A.; Naveh, D.; Towe, E. Tunable Band Gaps in Bilayer Transition-Metal Dichalcogenides. *Phys. Rev. B: Condens. Matter Mater. Phys.* **2011**, *84*, 205325.
44. He, K.; Poole, C.; Mak, K. F.; Shan, J. Experimental Demonstration of Continuous Electronic Structure Tuning *via* Strain in Atomically Thin MoS_2. *Nano Lett.* **2013**, *13*, 2931–2936.
45. Conley, H. J.; Wang, B.; Ziegler, J. I.; Haglund, R. F., Jr; Pantelides, S. T.; Bolotin, K. I. Bandgap Engineering of Strained Monolayer and Bilayer MoS_2. *Nano Lett.* **2013**, *13*, 3626–3630.
46. Enyashin, A. N.; Yadgarov, L.; Houben, L.; Popov, I.; Weidenbach, M.; Tenne, R.; Bar-Sadan, M.; Seifert, G. New Route for Stabilization of 1T-WS_2 and MoS_2 Phases. *J. Phys. Chem. C* **2011**, *115*, 24586–24591.